Published online 22 February 2018 *Nucleic Acids Research, 2018, Vol. 46, No. 8* ***3967–3980***
doi: 10.1093/nar/gky111

Human RAD51 rapidly forms intrinsically dynamic nucleoprotein filaments modulated by nucleotide binding state

Mário Špírek[1,2], Jarmila Mlčoušková[1,2], Ondrej Beláň[1], Máté Gyimesi[3], Gábor M. Harami[3], Eszter Molnár[3], Jiri Novacek[4], Mihály Kovács[3,*] and Lumir Krejci[1,2,5,*]

[1]Department of Biology, Masaryk University, Brno 62500, Czech Republic, [2]International Clinical Research Center, St. Anne's University Hospital Brno, Brno 65691, Czech Republic, [3]Department of Biochemistry, Eötvös Loránd University, Budapest H-1117, Hungary, [4]CEITEC, Masaryk University, Brno, Czech Republic and [5]National Centre for Biomolecular Research, Masaryk University, Brno 62500, Czech Republic

Received October 06, 2017; Revised February 01, 2018; Editorial Decision February 02, 2018; Accepted February 08, 2018

ABSTRACT

Formation of RAD51 filaments on single-stranded DNA is an essential event during homologous recombination, which is required for homology search, strand exchange and protection of replication forks. Formation of nucleoprotein filaments (NF) is required for development and genomic stability, and its failure is associated with developmental abnormalities and tumorigenesis. Here we describe the structure of the human RAD51 NFs and of its Walker box mutants using electron microscopy. Wild-type RAD51 filaments adopt an 'open' conformation when compared to a 'closed' structure formed by mutants, reflecting alterations in helical pitch. The kinetics of formation/disassembly of RAD51 filaments show rapid and high ssDNA coverage via low cooperativity binding of RAD51 units along the DNA. Subsequently, a series of isomerization or dissociation events mediated by nucleotide binding state creates intrinsically dynamic RAD51 NFs. Our findings highlight important a mechanistic divergence among recombinases from different organisms, in line with the diversity of biological mechanisms of HR initiation and quality control. These data reveal unexpected intrinsic dynamic properties of the RAD51 filament during assembly/disassembly, which may be important for the proper control of homologous recombination.

INTRODUCTION

Homologous recombination (HR) plays an essential role in repair of DNA double strand breaks (DSBs), stalled/collapsed replication forks and the generation of genetic diversity and proper chromosome segregation during meiosis (1). A crucial step in HR corresponds to the assembly of RAD51 NFs on ssDNA exposed at replication forks or nucleolytically-processed DSB ends. The NFs are capable of homology search and strand invasion into a sister chromatid, resulting in formation of a displacement loop (D-loop) structure. Subsequent processing of D-loops requires removal of the recombinase from DNA to allow repair synthesis using the homologous sequence as a template, followed by resolution/dissolution of recombination intermediates to complete repair (1).

Uncontrolled as well as erroneous HR can be toxic to the cell and is associated with genetic rearrangements, highlighting the importance of HR regulation. There is ample evidence that recombinase filaments represent a key platform for this regulatory control and the biological outcome of HR. Recombinases are a class of highly conserved proteins from bacterial RecA to yeast Rad51 (yRad51) and human RAD51. However, the mechanisms regulating recombinase NF assembly and activity differ greatly between species. In mammalian cells, BRCA2 is required for RAD51 nucleation (2), while other factors, such as the RAD51 paralogs, represent another class of positive effectors that remodel and stabilize NFs to promote recombinase activity (3,4). In contrast, negative regulators include helicases/translocases (RECQ5, FBH1, RAD54, RTEL1, HELQ, BLM) that either directly dismantle the NF or destabilize unscheduled and/or toxic RAD51-mediated intermediates (1,5).

Recent studies of RAD51 NFs indicate that the assembly process begins with a nucleation event, in which a small complex of 2–5 RAD51 monomers binds to the ssDNA (6–8). Additional subunits are added to the ends of the growing filament to form a long nucleoprotein polymer. Real time

*To whom correspondence should be addressed. Tel: +420 549493767; Fax: +420 549492556; Email: lkrejci@chemi.muni.cz
Correspondence may also be addressed to Mihály Kovács. Tel: +361 3722500/8401; Fax: +361 3812172; Email: mihaly.kovacs@ttk.elte.hu

experiments directly show that RAD51 multimeric species bind in a single kinetic step to ssDNA (8). Despite these insights the intrinsic properties of RAD51 filaments and the mechanistic insights into how HR regulatory factors influence recombinase filament formation/dynamics remain poorly defined.

In this study, using electron microscopy and DNA protection assays we revealed striking differences in human RAD51 NF pointing out to more 'open' WT filament conformation in contrast to relatively 'closed' K113R and K113A mutant filaments. This is manifested by dramatic changes of the helical pitch and representing dynamic features of NFs. For the first time we present rapid kinetic analysis of studied filaments in nanosecond time scale revealing complex kinetic behavior of human RAD51 filament assembly and disassembly and we interrogated the function of the ATPase active site of RAD51 and various nucleotide binding states. We further elaborated this analysis to yeast and bacterial recombinases highlighting important evolutionary mechanistic divergence among these proteins, reflecting the diversity of biological mechanisms of HR initiation and quality control. Establishing inherently dynamic properties of the RAD51-ssDNA interaction is a feature that could enable efficient remodeling and/or disassembly of NFs linked to dramatic conformational changes, thus providing novel insights into HR control. The importance of these observations is highlighted by mutations in RAD51 and its mediator proteins in genome instability disorders and cancer (1).

MATERIALS AND METHODS

Protein preparation

Human RAD51 protein was purified according to the previously published protocol, with few modifications (9). Expression plasmid pET11c-Rad51 was introduced into *Escherichia coli* BLR(DE3)pLysS cells (Novagen) and the culture was grown to A_{600} ~0.7 in 2 × TY media supplemented with ampicillin (100 mg/l) and chloramphenicol (33 mg/l). Expression of RAD51 protein was induced by the addition of IPTG (1 mM) at 37°C for 3–4 h, and cells were harvested at 5000 × g. Cells were then resuspended in cell breakage (CBB) buffer (50 mM Tris–HCl pH 7.5, 10% sucrose, 0.5 mM EDTA, 1 M KCl, 1 mM DTT and 0.01% NP-40, cocktail of protease inhibitors, and PMSF), were sonicated and centrifuged at 100 000 × g for 60 min. Clarified supernatant was mixed with ammonium sulfate (0.242 mg/ml) to precipitate RAD51 protein. After centrifugation of the mixture at 9000 x g, the pellet was resuspended in K buffer (20 mM K_2HPO_4 pH 7.5, 10% glycerol, 0.5 mM EDTA, 1 mM DTT and 0.01% NP-40) and loaded onto a Q Sepharose Fast Flow column (GE Healthcare) pre-equilibrated in K buffer supplemented with 175 mM KCl. The proteins were subsequently eluted with a gradient of 0.2–0.6 M KCl in K buffer. RAD51 peak protein fractions were pooled and loaded onto a hydroxyapatite (Sigma-Aldrich) column equilibrated with T buffer (25 mM Tris–HCl pH 7.5, 10% glycerol, 0.5 mM EDTA, 1 mM DTT and 0.01% NP-40) supplemented with KCl to 100 mM concentration. RAD51 was eluted by 60–260 mM KH_2PO_4 gradient in T buffer. Pooled peak fractions were loaded on Mono Q column (GE Healthcare) equilibrated with T buffer with 50 mM KCl. Protein was eluted with 200–450 mM KCl gradient in T buffer. Peak fractions were pooled and concentrated using Vivaspin Centrifugal Concentrator (30 000 MWCO PES). Aliquots were stored at –80°C. RAD51 ATPase mutants were purified using the same procedure and were tested for ATP binding and ATPase activity to confirm their status (Supplementary Figure S1A and B). Genes coding all RAD51 variants of expression plasmids were originally carrying 313Q mutation, which we corrected to 313K by site-directed mutagenesis and confirmed by sequencing. Yeast Rad51 protein was purified as described (10) and RecA protein accordingly to (11), alternatively was purchased from New England Biolabs (catalog number M0249).

Stopped-flow experiments and data analysis

Stopped-flow mixes were performed in SF50 buffer (50 mM Tris–HCl pH 7.5, 50 mM NaCl, 10 mM $MgCl_2$) at 25°C in a BioLogic SFM-300 instrument (at 1:1 volume mixing ratio and 1-ms dead time). Cy3 fluorescence was excited at 545 nm (4-nm bandwidth), and emission was monitored through a 550-nm longpass filter (Comar). HPLC-purified 5′-Cy3-dT_{79} and 3′-Cy3-dT_{79}, or dT_{79} oligonucleotides were purchased from VBC Biotech and Sigma. Postmix concentrations are stated throughout this article. Buffer-only and RAD51-free controls were included in all experiments. Controls in the absence of unlabeled dT_{79} were also included in dissociation kinetic experiments. All traces are shown normalized to the fluorescence level of RAD51-free 5′-Cy3-dT_{79} or 3′-Cy3-dT_{79}. Data analysis was performed using Origin 8.0 (Microcal Corp.). Kinetic modeling was performed to validate that the slope of the concentration-dependent k_{obs} profile in the suprastoichiometric [RAD51] regime ([RAD51] ≥ 1.5 μM) can be used as a reliable estimate for a second-order rate constant of association (k_{on}) (Supplementary Figure S2E and F).

EMSA

RAD51 protein or its mutant forms (final concentrations: 1, 2, 4 μM) was mixed with a master mix containing 5′-FITC-labeled 83-mer oligonucleotide (AAATGAACATAAAGTAAATAAGTATAAGGATA ATACAAAATAAGTAAATGAATAAACATAGAAA ATAAAGTAAAGGATATAAA) (1660 nM nt) in SF50 buffer with 1 mM ATP, in 10 μl reaction volume. Samples were resolved on 1% agarose gels in 1X TBE (70 V, 1 h 30 min) at 4°C. Gels were imaged on a FLA-9000 scanner (Fujifilm).

Nuclease protection assays

Proteins were diluted from concentrated stocks into T Buffer supplemented with 50 mM KCl, which was also used in no protein controls. Proteins were pre-incubated for 5 min on ice then mixed with 1830 nM (nucleotides) 5′- or 3′-fluorescein-labeled 61-mer oligonucleotide (GACGCTGCCGAATTCTACCAGTGCCTTGCTAG

GACATCTTTGCCCACCTGCAGGTTCACCC) in SF buffer in 10 μl reaction volume at 37°C for 10 min. Bovine pancreatic DNaseI (2 U, New England Biolabs) or S1 Nuclease (2 U, Thermo Fisher Scientific) was then added for 20 min at 37°C. The reaction was supplemented with 1 mM $CaCl_2$ in the case of DNaseI. The samples were deproteinized with 0.125% SDS and 12.5 μg proteinase K for 10 min at 37°C and resolved in 10% native polyacrylamide gels in 1× TBE (110 V, 50 min). Gels were imaged on a FLA-9000 scanner (Fujifilm) and quantified with Multi Gauge V3.2 (Fujifilm). After adjusting for background, the % protection was determined for all samples then normalized to the value for DNaseI minus. Average relative protection values from at least three experiments were determined.

Electron microscopy

The RAD51–ssDNA complexes were formed in buffer containing 50 mM Tris–HCl pH 7.5, 50 mM NaCl, 10 mM $MgCl_2$ and 1 mM ATP or AMP-PNP, respectively. 5.4 μM protein was mixed with 16.2 μM ssDNA 150-mer (concentration in nucleotides) and incubated for 10 min at 37°C. The ssDNA 150-mer oligonucleotide was purchased from VBC Biotech.

Four microliter of sample was deposited on glow-discharged grids coated with 12 nm layer of homemade continuous carbon and stained with Nano-W (Nanoprobes Inc.). Alternatively, glow-discharged holey carbon Quantifoil R2/1 (200 mesh) TEM grids were used for preparation of cryo-EM samples. Data were collected on transmission electron microscope Tecnai F20 (FEI) operating at 200 keV with a nominal magnification of 50 000× resulting in pixel size of 2.22 Å/px. The data were acquired on CCD camera (FEI Eagle) under low-dose conditions (∼25 $e^-/Å^2$ s) and with the underfocus in the range of 2.5–4.5 μm. Altogether, 167 images were collected for RAD51wt-ssDNA filaments in presence of ATP, 390 images were collected for RAD51 WT-ssDNA filaments in presence of AMP-PNP, 255 images were collected for KR-ssDNA filaments, and 58 images were collected for KA-ssDNA sample. In cryo-EM, 506 images were collected for RAD51 WT and 370 images for KA filaments formed on ssDNA.

The contrast transfer function parameters were estimated using program ctffind4 (12). Micrographs were manually screened for presence of significant drift and astigmatism and filaments from selected micrographs were collected and extracted (box size 140 pixels for filaments formed by wild-type RAD51, 120 pixels for the rest) using e2helixboxer.py within EMAN2 software package (13). The particles were reference-free classified using RELION-2.0 (14) and only classes representing straight segments of the helix were selected for further analysis. Selected particles were refined using IHRSR (15) protocol within RELION-2.0. Helical parameters previously published for human RAD51 filaments (16) were used as starting values during the refinement of all structures. The three-dimensional models were visualized in UCSF Chimera (17). Filament lengths were evaluated using manual tracking tool in ImageJ (18).

RESULTS

RAD51 filament structure is strongly influenced by the properties of that RAD51 nucleotide binding site

We sought to interrogate structural and dynamic properties of RAD51 NFs and to further define how these structures are altered by nucleotide binding. We first employed electron microscopy (EM) of NFs using negative stain with Nano-W (methylamine tungstate), which is less structurally damaging and more pH-friendly than conventional EM methods employed previously (16). The EM visualization and reconstruction of various RAD51 filaments in the presence of ATP revealed striking structural differences reflected by dramatic changes in the helical pitch of the NFs (Figure 1). The observed symmetry of 6.3 units/turn and pitch 108 Å (negative stain) associated with an 'open' wild-type (WT) filament conformation. This finding is in agreement with values previously reported for yRad51 filaments formed on dsDNA in the presence of ADP and AlF_4^- anions (19) and human RAD51 filaments formed on ssDNA in the presence of ADP and AlF_4^- anions (16) or AMP-PNP (a non-hydrolyzable ATP analog) (20,21), respectively. We next tested RAD51 Walker box mutants known to be defective in either ATP hydrolysis (RAD51 K133R (KR)) or ATP binding (RAD51 K133A (KA)) (22). The 3D reconstructions of both KR and KA mutants with ATP and WT RAD51 in the presence of AMP-PNP, revealed a 'closed' structure with average pitch ranging from 71 to 80 Å (Figure 1 and Supplementary Figure S1A). Similar values for the pitch (∼76 Å) were reported for RAD51 filaments formed on ssDNA in the presence of ATP-γ-S cofactor (16). To assess the influence of Nano-W staining on the NF structure, two control samples were also evaluated using cryo-EM microscopy. No significant differences in helical parameters were observed between EM and cryo-EM experiments in case of the KA mutant, while slightly higher values of the pitch were obtained for the WT filaments in presence of ATP (Figure 1 and Supplementary Figure S1A).

Statistical analysis of RAD51 WT incubated with ATP showed an average filament length of 71 nm (Supplementary Figure S1B). This corresponds to the theoretical length of a 150-nt ssDNA extended by a factor of ∼1.5 compared to the length of B-form DNA (19) and is in agreement with previously published data for RAD51 filaments (23). Accordingly, the peak maximum filament length observed for RAD51 WT in the presence of AMP-PNP as well as for the KR and KA mutants lies between ∼39 and 44 nm (Supplementary Figure S1B), further supporting compressed 'closed' properties of these filaments. Additional peaks likely correspond to end-to-end stacking of two or three filaments (19,24). During our analysis Xu et al. 2017 published a study where RAD51 forms extended filament structures in AMP-PNP presence (21). To elucidate this contradictory observation we repeated the EM study using their conditions and even using Nano-W stain we observed filaments with pitch 104 Å (Supplementary Figure S1E). Given the effect of various salt, buffers, nucleotides and their concentrations affecting the RAD51 filament it is therefore essential to provide biochemical, biophysical and structural analysis under comparable conditions.

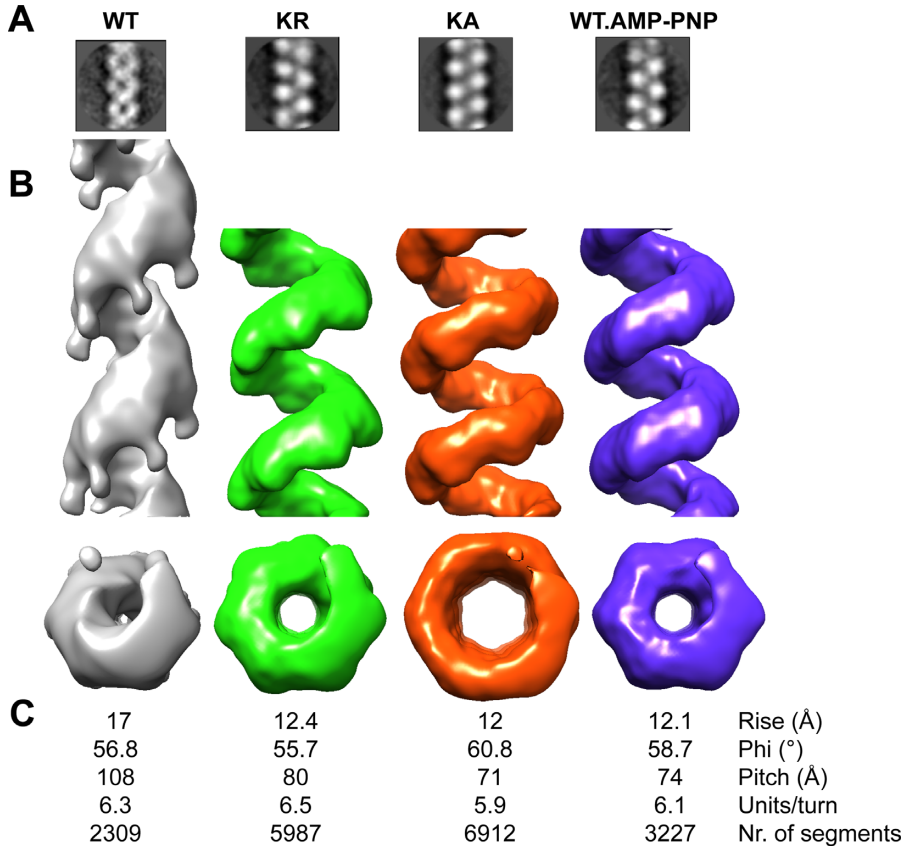

Figure 1. EM analysis of human RAD51 filaments. (**A**) Representative class-averages and (**B**) three-dimensional reconstructions of human RAD51 WT, KR and KA filaments formed on short single-stranded DNA (150-mer) in the presence of ATP and wild-type in the presence of AMP-PNP. Approximately two turns of the filament are shown and the class-average box size is 140 pixels for the WT in the presence of ATP and 120 pixels for the rest. (**C**) Calculated helical parameters from reconstructions of individual NFs are depicted.

Since the EM data revealed dramatic structural changes of RAD51 Walker box mutants relative to WT, we used electrophoretic mobility shift (EMSA) analysis to monitor the mobility of NFs in agarose gels. Incubation of RAD51 or its mutants with ssDNA in the presence of ATP revealed significant differences in the migration of protein–DNA complexes in the presence of ATP (Figure 2A). Specifically, both KR and KA mutants form slower migrating complexes compared to wild-type protein filaments. Interestingly in the case of KA mutant, a fast migrating complex can also be detected, probably reflecting a transient form of filament. This altered mobility may reflect the 'open' and 'closed' conformations of NF observed in EM experiments described above. To further probe the structural differences between NFs we used nuclease protection assays with DNaseI, which we have employed previously to study structural alterations in the *C. elegans* RAD-51 filament upon remodeling by the Rad51 paralogs (3). In agreement with a more open conformation, RAD51 WT filaments display a markedly different digestion pattern, with 3–4-fold higher accessibility of DNA to DNaseI digestion compared to both Walker box mutants (Figure 2B). Although we used in the nuclease assay high concentration of magnesium ions, low concentration of calcium necessary for DNaseI activity could affect the filament behavior. Nevertheless, using S1 nuclease that does not require Ca^{2+} ions we observed the same result (Supplementary Figure S1F). Similar dramatic effects were observed when AMP-PNP analog was used in the reaction with WT RAD51, supporting the view that the lower helical pitch observed in EM likely presents a steric barrier to nuclease activity (Figure 2C). Collectively, our data reveal distinct structural changes in the RAD51 filament associated with ATP binding and hydrolysis.

RAD51 displays rapid ssDNA binding kinetics in a multistep process

To characterize the molecular basis of RAD51 NF structural differences, we performed kinetic studies of filament formation and dissociation. The interaction of RAD51 with ssDNA was monitored using a Cy3 fluorescent moiety (25) placed at the 5′ end of oligo-dT_{79} (5′-Cy3-dT_{79}). This assay has previously revealed a large protein-induced fluorescence increases upon interaction with yRad51 and nematode RAD-51 (3,26). In stopped-flow experiments we rapidly mixed a constant concentration of 5′-Cy3-dT_{79} (40 nM molecules; 3160 nM nucleotides) with increasing concentrations of RAD51 (0.5–5 μM monomers) (Figure 3B and Supplementary Figure S2) to assess the reactions in both sub- and supra-stoichiometric regimes with regard to the protein/ssDNA concentration ratio. The stopped-flow methodology allowed us to monitor the Cy3 fluorescence

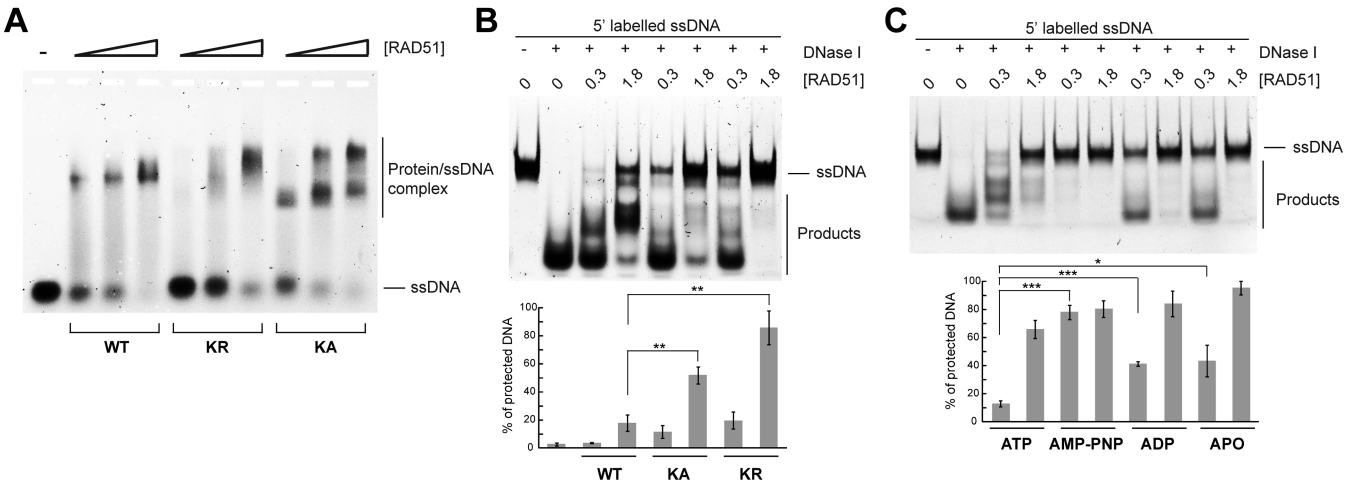

Figure 2. Structural properties of human RAD51 nucleofilaments. (**A**) The mobility of RAD51 NF is influenced by Walker box mutations. Binding of individual RAD51 proteins (1, 2, 4 μM) to ssDNA (83-mer, 1.66 μM nt) was monitored by EMSA. (**B**) DNaseI protection assay on protein-DNA complexes formed by RAD51 and walker box mutants with ssDNA in the presence of ATP. (**C**) DNaseI protection assay on RAD51 NFs in the presence of indicated nucleotides. Errors bars indicate S.D. ($n = 3$).

signals in the time frame ranging from 1 ms to 60 s (Figure 3A). To assess the effect of nucleotide bound to the ATPase active site, we used proteins either free of nucleotide (apo) or pre-incubated with 1 mM ATP, ADP or AMP-PNP prior to mixing with ssDNA. The recorded association transients showed very rapid filament formation that reached apparent completion within 1s (Figure 3A and B). These transients displayed multiphasic properties and could be fitted with three exponentials (Supplementary Figure S2A–D, Eq. S1), suggesting a complex assembly mechanism, possibly occurring in several phases. We used the total amplitudes of the reaction transients to estimate the equilibrium binding properties, using a quadratic binding equation with apparent RAD51:ssDNA binding affinity and stoichiometry as floating parameters (Figure 3B, Eq. S2). By this analysis, upper limits for apparent K_d values were detected to be below 1 μM (Supplementary Table S1). We note that this simplified analysis, used to verify the ssDNA binding capability of RAD51, assumes binding of independent RAD51 units (with no assumption on oligomeric state) along the DNA lattice.

To further understand the mechanism of filament formation, we applied linear fits to the RAD51 concentration dependence of observed rate constants (k_{obs} values) of each phase (Supplementary Figure S2D). This analysis provided slopes (apparent k_{on} values) and intercepts (apparent k_{off} values) (Supplementary Figure S2G) for all kinetic phases (Supplementary Figure S2D; analysis results shown in Figure 3C). Based on these results, two possible models of the multiphasic RAD51-ssDNA binding kinetics can be suggested: (i) a 'sequential' binding mechanism in which an initial second-order association phase is followed by successive first-order isomerizations of the RAD51-ssDNA complex, or (ii) a 'parallel' mechanism in which a pre-existing heterogeneity within the DNA-free RAD51 population interacts with ssDNA with different second-order association and first-order dissociation rate constants (k_{on} and k_{off} values, respectively). For the second-order association phase, the slope and intercept of the linear k_{obs} as a function of RAD51 concentration reflects the k_{on} and k_{off} values, respectively (Supplementary Figure S2E–G). Whereas for a first-order isomerization phase, k_{obs} is expected to show saturation with increasing RAD51 concentration, and its saturating value reflects the sum of the forward and reverse rate constants of the isomerization step. Thus, multiple kinetic phases with significant slopes (and relatively small or zero intercepts) indicate parallel binding steps with weak or strong affinity, whereas kinetic phases with zero slope (or a high intercept/slope ratio (>>1 μM)) indicate first-order isomerizations (Supplementary Figure S2G). Second-order steps with very low affinities are unlikely to be discernible in the kinetic profiles. Our data indicate that filaments formed in the presence of ATP undergo two consecutive isomerization reactions after the initial binding step (Figure 3C). The comparison of this profile to those with either AMP-PNP or ADP (Figure 3C) suggests that at least one of the isomerization phases with ATP is driven by ATP hydrolysis. Interestingly, AMP-PNP drives strong RAD51 binding to ssDNA with no isomerization detected (Figure 3C). This might correspond to nucleotide-dependent changes in the oligomeric state of the protein (27) and the nucleation sites formed on ssDNA. As it was shown that calcium ions activate RAD51 by modulating its ATPase activity, we replaced magnesium ions with 1 mM calcium, the concentration with strongest effect on D-loop formation (28). The presence of calcium clearly mimics AMP-PNP conditions and drives RAD51 to strong binding mode and thus reduced ATPase activity correlates with loss of isomerization (Figure 3C).

To further assess the role of nucleotide cofactor binding/hydrolysis on the formation of RAD51 filaments, we analyzed NF assembly kinetics of the KA and KR mutants. The assembly kinetic profiles of these mutants showed characteristic differences from those of the WT protein (Figure 3C and Supplementary Figure S3). In the absence of nucleotide, KR displays assembly kinetics in general similar to WT, whereas in the presence of ATP it resembles those

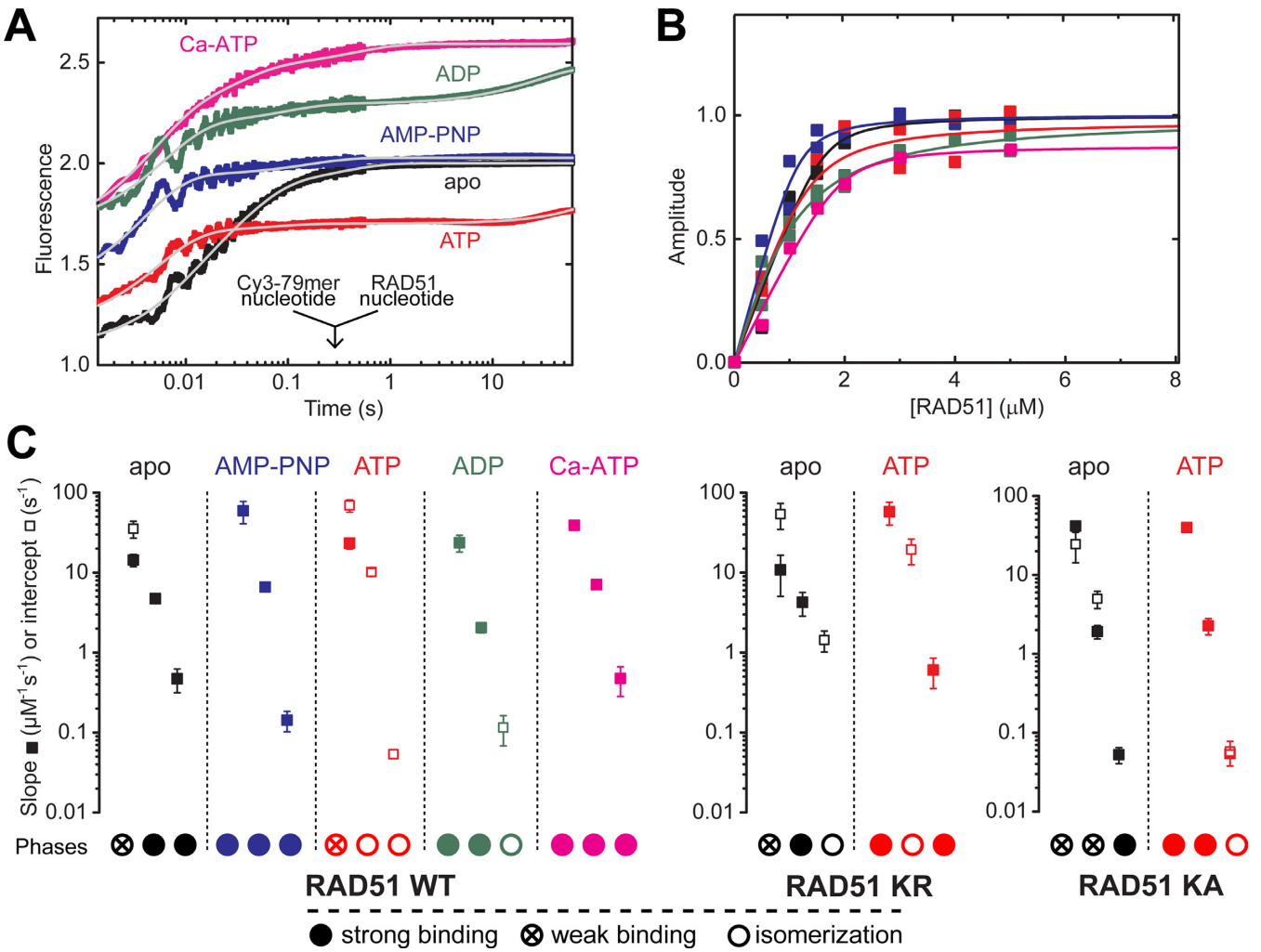

Figure 3. Rapid kinetics of RAD51 filament formation. (**A**) Effect of nucleotides or calcium ions (1 mM; as indicated) on RAD51 (recorded at 5 μM recombinase concentration) filament formation on ssDNA (40 nM 5′-Cy3-dT_{79}) monitored by fluorescence signal change in stopped-flow. Tri-exponential best-fits (Eq. S1) are shown as gray lines. (**B**) RAD51 concentration dependence of recorded total fluorescence changes is shown relative to the extrapolated maximal amplitude of individual datasets. K_d values (determined from quadratic fits (solid lines) based on Eq. S2) are listed in Supplementary Table S1. (**C**) Association kinetic parameters for RAD51 WT, KR and KA (shown with horizontal offsets) were determined from linear fits in Supplementary Figure S2D applied to protein concentration (in the ≥1.5 μM range) of individual observed rate constants (k_1, k_2 and k_3). Slopes (solid squares) are plotted if significantly different from 0. Intercepts (open squares) are plotted, except if the slope was significantly different from 0 but the intercept was not (e.g. RAD51.AMP-PNP). Error bars show standard errors of global fits to all rate constant data of a given kinetic phase. Consecutive phases at given condition are indicated by circles. Strong binding (solid circle): significant slope, zero intercept. Weak binding (crossed circle): both the slope and intercept are significantly different from 0. Isomerization (empty circle): slope is not significantly different from 0.

of WT with AMP-PNP or ADP (Figure 3C). However, one isomerization phase was also observed for the KR mutant. Unexpectedly, KA filament assembly, both in the absence of nucleotide and with ATP, is similar to that of WT RAD51 in the presence of AMP-PNP or ADP (Figure 3C), indicating that this Walker box mutation mimics nucleotide cofactor-bound WT RAD51. Notably, the small response of KA to the addition of ATP reflects its weak nucleotide cofactor binding properties (29). Taken together, these findings indicate that NF assembly occurs through random and independent binding of RAD51 units along ssDNA, and is intimately related to nucleotide-mediated changes of protein structure.

RAD51–ssDNA filaments show dynamic heterogeneity

Although RAD51 NF assembly represents a crucial step in HR promotion, factors such as antirecombinases can actively prevent HR by a disruption of NF (30,31). Failure to stabilize RAD51 NF by C-terminally truncated BRCA2 variants leads to elevated replication stress through enhanced nascent DNA strand degradation (32), thereby contributing to cancer development. Hence, we have investigated the kinetic stability of NFs by challenging them with excess of unlabeled competitor ssDNA in various conditions to monitor the dissociation of RAD51 molecules from labeled ssDNA.

To this end, we preincubated RAD51 WT, KR or KA (0.5–5 μM) for 5 min in the absence or presence of the individual nucleotides (1 mM) as in the association kinetic

experiments (see above), followed by incubation with 5′-Cy3-dT_{79} (40 nM molecules, 3.16 μM nt) for 15 min to form steady-state NFs. To monitor dissociation kinetics, we rapidly mixed these complexes with a large excess of unlabeled dT_{79} (4 μM molecules, 316 μM nt) to sequester any RAD51 released from labeled ssDNA molecules (Figure 4). To assess how the ssDNA coverage fraction affects the dissociation transients, we performed the experiments at 0.5 and 5 μM of individual proteins, resulting in partial and full coverage of dT_{79} molecules, termed 'disperse' and 'saturated' conditions, respectively (D and S in Figure 4B).

Similar to NF assembly, the kinetics of RAD51 dissociation from ssDNA generally produced multiexponential profiles (Figure 4, evaluated using Eq. S1), suggesting a complex disassembly mechanism. While in the apo form only one kinetic phase was detected, addition of different nucleotides resulted in multiple dynamic fractions (Figure 4B), indicating the heterogeneous nature and/or multiple intermediate states of RAD51 filaments during disassembly. The calcium ions greatly stabilized the filaments with only single-exponential dissociation behavior distinguishing it from AMP-PNP and suggesting its possible role in regulation. To exclude the possibility that the multiphasic dissociation profiles result from partial saturation of RAD51 active sites with nucleotide, we performed ATP titration experiments. The results of these experiments show that RAD51 saturation is already achieved at 25 μM ATP concentration (Supplementary Figure S4). In all cases the residual fluorescence level after the detected dissociation phases (60 s) is significantly higher than that of 5′-Cy3-dT_{79} alone, suggesting that a large fraction of RAD51 molecules remained stably bound to ssDNA with lifetimes longer than the observation period (Figure 4B). This was also confirmed in control experiments performed with bacterial SSB, human RPA and yeast Srs2 proteins in place of RAD51 (Supplementary Figure S5).

Experiments with KR and KA in the absence of nucleotide showed more dynamic dissociation profiles as those observed for WT RAD51 in the apo state. In particular, the appearance of highly dynamic fractions with lifetimes below 1 s was observed for KA (Figure 4B). Similarly, the profile of both mutants with ATP was also more dynamic and complex due to a presence of an extra fraction, compared to WT RAD51 in the nucleotide-bound state under saturated conditions (Figure 4B). However, in disperse conditions KR mutation produces a larger fraction of stable NFs, confirming its observed *in vitro* stability (22). Taken together, these experiments show that alterations in the RAD51 Walker box motif diminish the impact of ATP binding/hydrolysis on NF stability.

Since previous studies have observed both bidirectional recombinase filament growth (33) and unidirectional RAD51 filament growth in the presence of BRCA2 (34), we measured the intrinsic preference of RAD51 towards polar filament growth. To this end, we performed the above association and dissociation kinetic experiments using dT_{79} labeled at its 3′ terminus (3′-Cy3-dT_{79}) and compared them with reaction profiles recorded using 5′- labeled DNA (5′-Cy3-dT_{79}) in the presence or absence of ATP. Overall, the position of the Cy3 label did not convey a large effect on the amplitude and rate constant profiles of the reactions (Supplementary Figure S6 and Supplementary Table S1). Furthermore, the isomerization phases of NF formation in the presence of ATP were detected with both 5′- and 3′-labeled DNA, suggesting this process occurs throughout the entire length of the filament (Supplementary Figure S6B). We observed slightly faster dissociation kinetics at the 3′ compared to 5′ end in the absence of nucleotide, as indicated by the appearance of a short-lived fraction, pointing to enhanced NF stability toward the 5′ end (Supplementary Figure S6D).

The effect of ATP on preassembled RAD51-ssDNA filaments

In all of the above rapid kinetic experiments, nucleotide cofactors were incubated with RAD51 prior to mixing RAD51 with ssDNA to mimic the physiological scenario of nucleotide-bound RAD51 engaging with DNA. However, the capability of nucleotide-free RAD51 to form complexes with ssDNA allowed us to address the possible mechanistic effect of ATP on preassembled RAD51-ssDNA filaments. Therefore, we assessed reaction profiles upon rapidly mixing nucleotide-free RAD51 with a pre-mixture of 5′-Cy3-dT_{79} (or 3′-Cy3-dT_{79}) containing increasing concentrations of ATP. We found that the post-mixing addition of ATP resulted in the appearance of a slow fluorescence decrease phase (Supplementary Figure S7A). The ATP concentration dependence of the amplitude and k_{obs} values of this phase was indicative of an apparent single-step reaction, corresponding to slow but strong binding of ATP to preformed RAD51-ssDNA complexes, with the maximal amplitude already reached at 250 μM ATP (Supplementary Figure S7B and C). The kinetics of this process was largely unaffected by either the position of the Cy3 label, the KR mutation or by replacement of magnesium by calcium ions (Supplementary Figure S7B–D). As expected, the ATP-binding deficient KA mutant did not show significant ATP interaction (Supplementary Figure S7D). We also performed the experiments with yRad51 under identical conditions. While RAD51 showed rapid ssDNA binding followed by slow ATP association with the RAD51-ssDNA complex, ssDNA binding by yRad51 is slow and weak in the absence of ATP, but markedly accelerated in the presence of ATP (Supplementary Figure S7D). These results imply rapid ATP binding to yRad51 that precedes and enhances the binding of the protein to ssDNA, highlighting a striking difference from the human protein, where binding to ssDNA precedes the binding to ATP.

Evolutionary comparison of recombinases

To further compare the evolutionary conservation of these processes we purified bacterial RecA and yeast Rad51 recombinases and assessed their kinetic profiles in the above-described NF assembly and disassembly setups. Similar to human RAD51, the ssDNA association amplitude profiles of RecA also showed binding with apparent K_d values below 1.1 μM and apparent binding stoichiometries in line with 3 nt/monomer for all nucleotide states assessed (Supplementary Table S1). In contrast, yRad51 exhibited a striking nucleotide dependence with very weak binding in

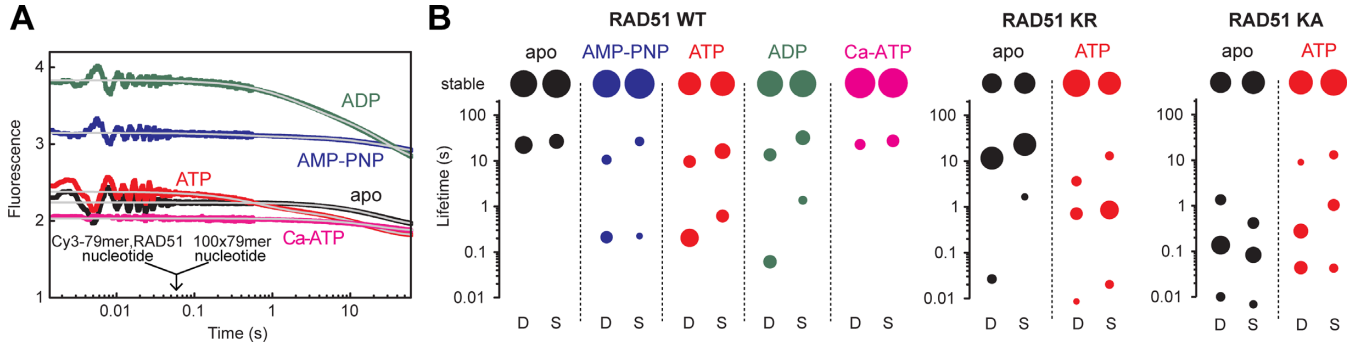

Figure 4. Rapid kinetics of human RAD51 dissociation from ssDNA. (**A**) RAD51 (5 μM) was preincubated with 40 nM (3.16 μM nt) 5′-Cy3-dT_{79} in the absence (apo) or presence of the indicated nucleotides (1 mM), and rapidly mixed in the stopped-flow with 4 μM (316 μM nt) unlabeled dT_{79} (post-mixing concentrations stated). Transient Cy3 fluorescence levels are shown relative to that of RAD51-free 5′-Cy3-dT_{79}. Multi-exponential best-fits (Eq. S1) are shown in grey. (**B**) Lifetime components of dissociation transients of RAD51 WT, RAD51 KR and RAD51 KA. Distribution of lifetimes ($\tau_i = 1/k_i$ values, cf. Eq. S1) of dissociation transients recorded in (A) under 'disperse' (D, 0.5 μM RAD51) and 'saturated' (S, 5 μM RAD51) conditions. Areas of symbols are proportional to fractional amplitudes of the individual phases (A_i values, cf. Eq. S1). Results are shown as average values for two datasets.

the apo state, cooperative binding in the AMP-PNP state, and strong binding in the presence of ATP (Figure 5A–D and Supplementary Table S1). Similarly to RAD51, the recorded association transients were multiexponential in all cases, and could be well fitted with three exponentials (Figure 5E and F), supporting the similarity of the underlying mechanism of NF assembly.

We also performed dissociation experiments with yRad51 and RecA. Interestingly, yRad51 appeared almost entirely stably bound in apo and AMP-PNP, showed some dynamic heterogeneity with ATP, and a significant fraction of short lifetime state with ADP (Figure 6B and D), suggestive of a role for ATP hydrolysis in filament dissociation. However, the stability of apo-yRad51 NFs could not be properly evaluated due to the low level of ssDNA binding (Figure 5D). The RecA filaments show striking differences from both yeast Rad51 and human RAD51, due to the appearance of a large and short-lived fraction in the apo, AMP-PNP, and ADP-bound states (Figure 6, cf. Figure 4). Previously published data have suggested that RecA filaments more stably nucleate on the ssDNA in the presence of non hydrolysable ATP analog ATPγS (35). In our set-up the observed AMP-PNP effect could be attributed due to either different binding mode or the increased dynamics of RecA filaments, which we detect in all nucleotide states. Furthermore, RecA NFs are unstable, but show increased stable fractions in all tested conditions when present in saturated concentrations (Figure 6A and C), indicating higher stability due to strong neighbour-joining stabilizing effect. In this context, human RAD51 NF are stabilized by a different mechanism, since the amount of stable fraction remains generally unchanged but their lifetimes are longer in saturated conditions (Figure 4B). In general, the dissociation of human RAD51 NFs appears more complex in all nucleotide-bound states in particularly compared to yRad51.

DISCUSSION

RAD51 filament formation represents an essential step during repair of DSBs and the protection of stalled replication forks. By direct visualization and 3D reconstruction we determine the existence of striking structural changes between various RAD51 NFs. We define an 'open' conformation for the WT filament in the presence of ATP, which contrasts with a 'closed' conformation observed with AMP-PNP or RAD51 Walker box mutants, K113R and K113A. These distinct structural states reflect dramatic changes in the helical pitch and rise and could represent different intermediate states during the dynamic process of RAD51 filament formation, in which ATP-binding/hydrolysis-deficient NFs are locked. Notably, the structural changes in the NFs induced by nucleotide or Walker box mutants were also detected by nuclease protection assays and EMSA.

To help further understand the mechanistic properties behind these conformational changes together with general features of RAD51 filament assembly in real-time we performed rapid kinetic analyses. We show an unappreciated ability of RAD51 to bind ssDNA and form filaments through a multistep process over a millisecond time-scale using short fluorescently labeled ssDNA. Based on our data we propose a model of RAD51 DNA binding, where initial quasi-independent binding of RAD51 units along the DNA ensures rapid ssDNA coverage. Subsequently, a series of isomerization events creates a compressed ''closed' filament that can be converted in an ATP-dependent manner to an extended 'open' filament (Figure 7). We also observed changes in the association kinetics in relation to various nucleotide states and Walker box mutations. We hypothesize that this could be attributed not only to observed structural changes, but also to the oligomeric state of the protein (27) and/or multiple nucleation sites on ssDNA. While large oligomers could cover a large portion of ssDNA in one binding step, leading to formation of regular (continuous) filaments, small oligomers could form several nucleation sites that could result in irregular filaments containing small gaps. Such irregularities would require subsequent isomerizations to adopt a regular contiguous filament. Similar behavior has been described for RecA filaments in the presence of ATPγS where isomerization leads to changes between rigid and flexible filaments (36,37). Our hypothesis is in line also with recent data showing that RAD51 filaments grow from a stable heterogeneous nuclei ranging in size from dimer (8,38) and perhaps even monomers to

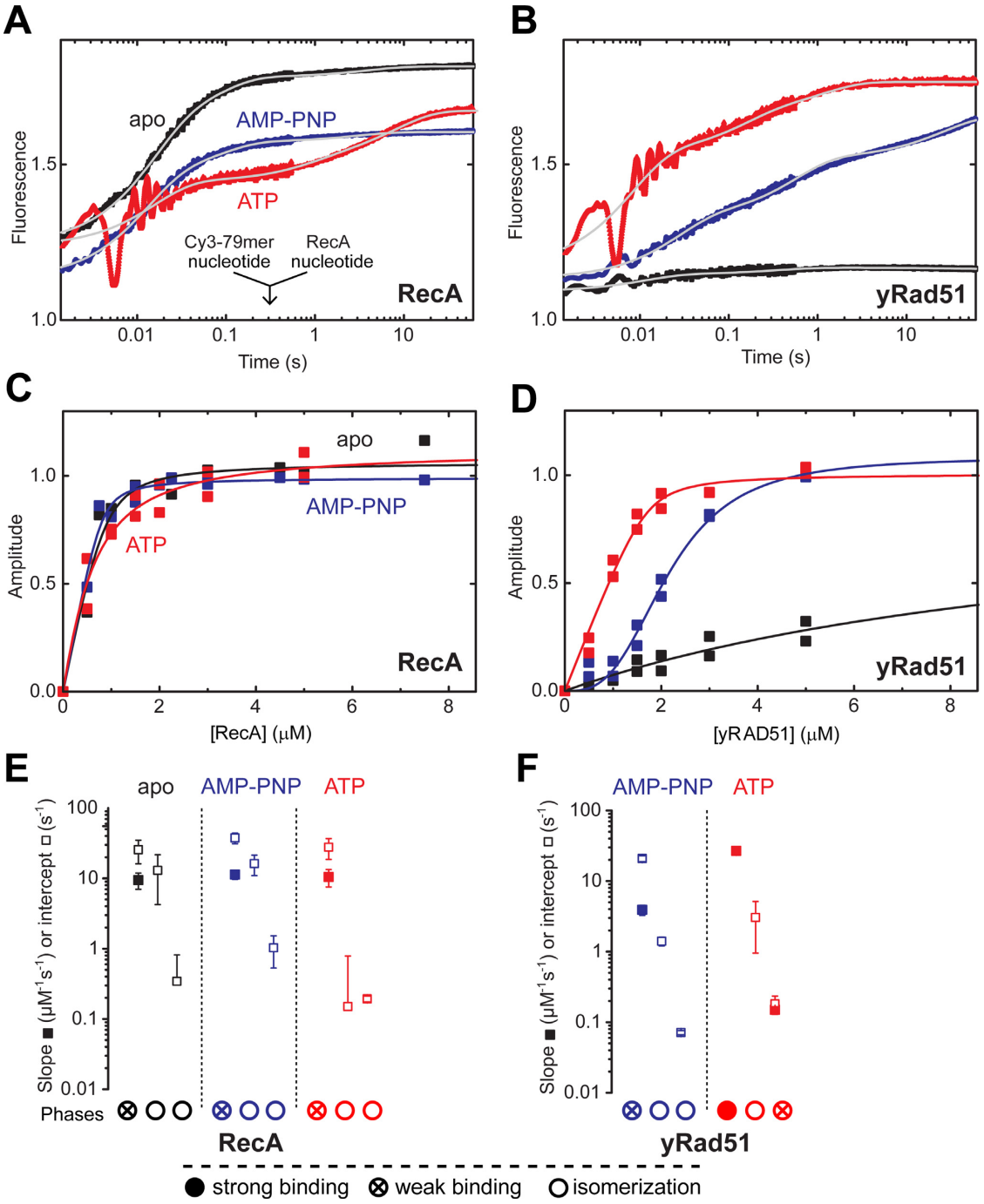

Figure 5. The evolutionary comparison of the ssDNA association kinetics of bacterial and yeast recombinases. Effect of nucleotides (apo, black; AMP-PNP, blue and ATP, red (1 mM) on recombinase NF formation, recorded by mixing 5 μM RecA (**A**) and yRad51 (**B**) with 40 nM 5′-Cy3-dT_{79}. Tri-exponential best-fits (Eq. S1) are shown as gray lines. (**C**) RecA and (**D**) yRad51 concentration dependences of recorded total fluorescence changes are shown relative to the extrapolated maximal amplitudes of individual datasets. K_d values (determined from quadratic fits (solid lines) based on Eq. S2) are listed in Supplementary Table S1. Association kinetic parameters for (**E**) RecA and (**F**) yRad51 (shown with horizontal offsets) were determined as in Supplementary Figure S2D (cf. Figure 3C). Slopes (solid symbols) are plotted if significantly different from 0. Intercepts (open symbols) are plotted, except if the slope was significantly different from 0 but the intercept was not. Error bars show standard errors of global fits to all rate constant data of a given kinetic phase. Consecutive phases at given condition are indicated by circles (cf. Figure 3C).

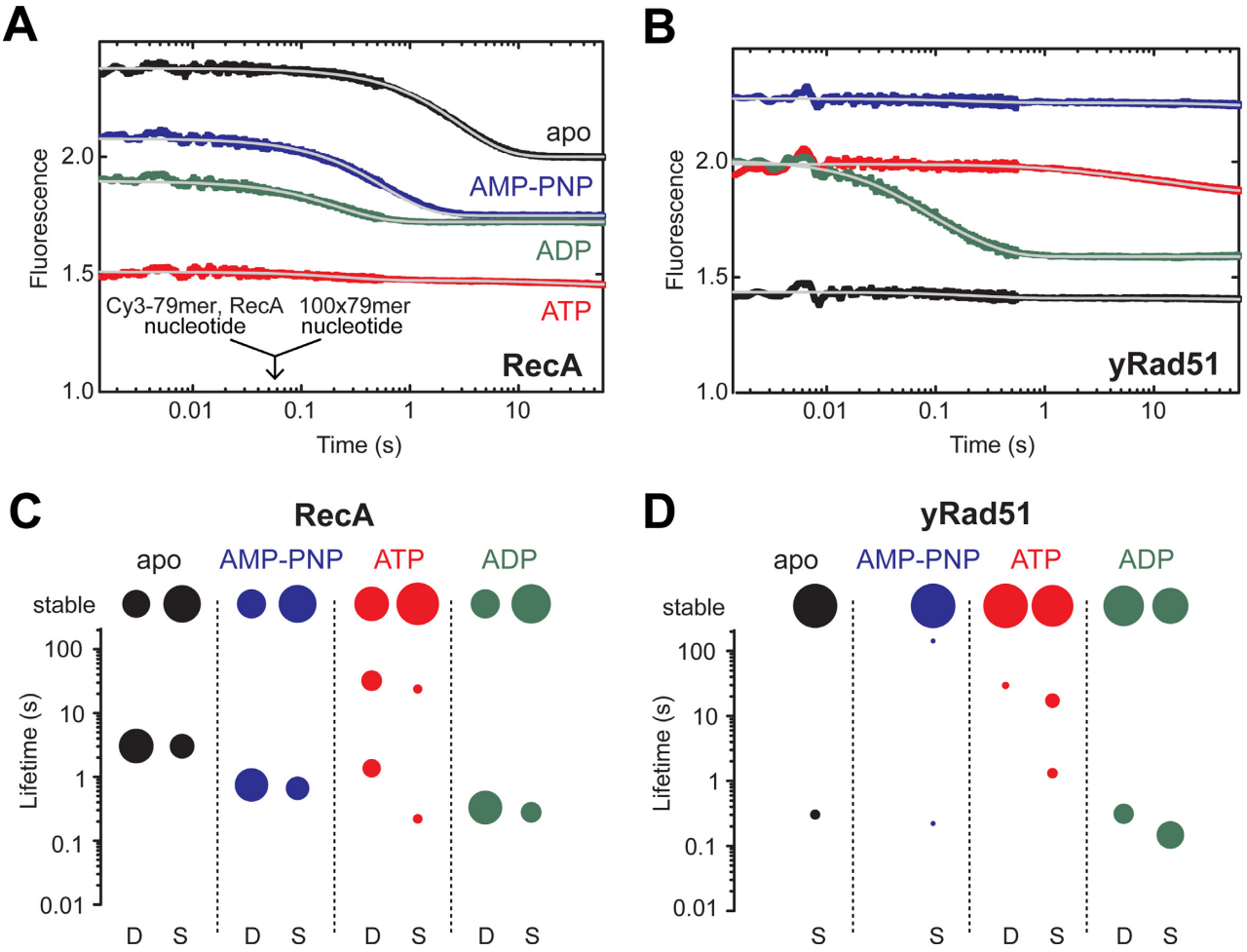

Figure 6. The evolutionary comparison of RecA and yRad51 NF dissociation kinetics. (**A**) RecA or (**B**) yRad51 was preincubated in the absence (apo) or presence of the indicated nucleotides (1 mM) with 40 nM (3.16 μM nt) 5′-Cy3-dT$_{79}$, followed by rapid mixing in the stopped-flow with 4 μM (316 μM nt) unlabeled dT$_{79}$ (post-mixing concentrations stated). Transient Cy3 fluorescence levels of RecA or yRad51 are shown relative to that of recombinase-free 5′-Cy3-dT$_{79}$. Multi-exponential best-fits (Eq. S1) are shown in grey. Lifetime components of RecA (**C**) and yRad51 (**D**) dissociation transients. Distribution of lifetimes ($\tau_i = 1/k_i$ values, cf. Eq. S1) of dissociation transients recorded in (A and B) under 'disperse' (D, 0.5 μM recombinase) and 'saturated' (S, 5 μM recombinase) conditions are shown (cf. Figure 4B). Areas of symbols are proportional to A_i values (cf. Eq. S1). Results are shown as average values for two datasets.

large oligomers (8). Moreover irregular human RAD51 filaments were detected on long ssDNA substrates using scanning force microscopy (39).

Similar events could also serve to regulate filament disassembly, as our data uncover the complex nature of RAD51 NF dissociation characterized by the presence of different species and/or multiple consecutive steps (Figure 7). The dissociation of NFs is influenced by nucleotide binding state or mutations in the ATP-binding Walker motif. This motif has undeniably a crucial role in RAD51 filament regulation. While KR mutation increases strand-exchange and stabilizes NFs, the KA mutation has the opposite effect (22). Interestingly, we show that these alterations in the RAD51 Walker box motif not only diminish ATP binding/hydrolysis, but also affect NF stability by a nucleotide cofactor-independent manner, which likely reflect structural difference in the NFs as demonstrated by EM. Since KA mutant is incapable of strand exchange activities *in vitro* in contrast to KR mutant, the change in the helical pitch is not the only requirement for the activity of RAD51 in the cell. Nucleotide-free KA is particularly interesting as its kinetic parameters resemble those of nucleotide-bound WT RAD51. Intriguingly, recent data imply that the Walker box mutants show very similar phenotypes *in vivo* including replication defects and effects on protein dynamics (40). This indicates that improperly assembled NFs and their dynamics could lead to impaired homology search *in vivo* and/or an inability to be activated/protected in a response to RAD51-interacting recombination mediators. Moreover, single molecule data showing dynamic rearrangements of NF (39) and the process of RAD51 NF nucleation occurring through a dynamic binding (38) support our observations.

We imply that the heterogeneous nature, multiple intermediate states and structural changes within NFs might promote more efficient homology search. Firstly, this HR step requires a complex interplay between recombinases, presynaptic ssDNA, homologous dsDNA template, in the

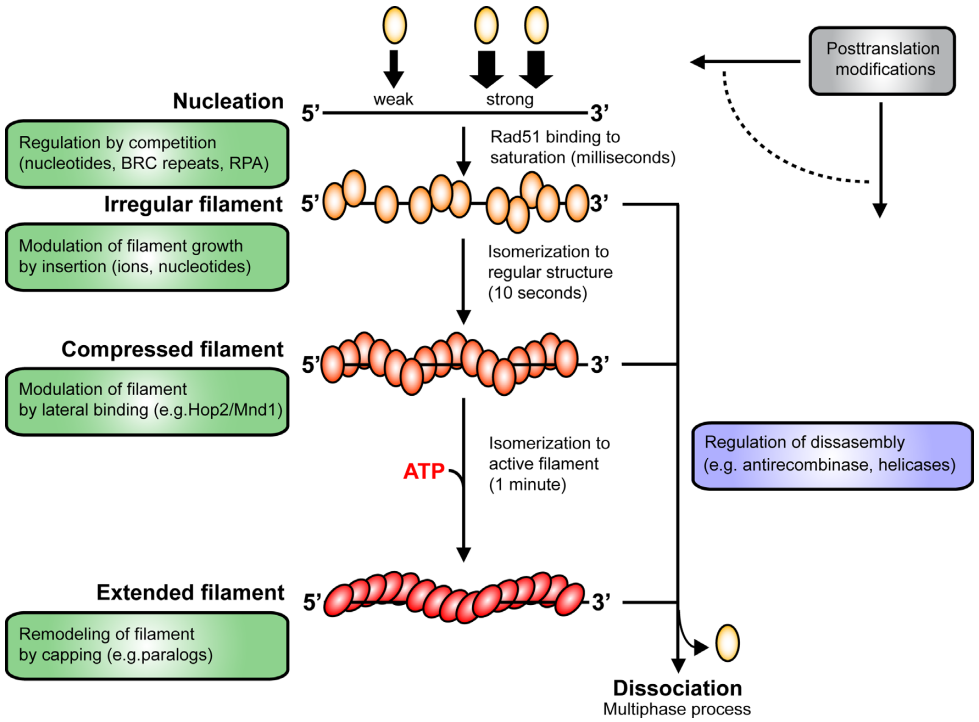

Figure 7. Schematic model representing formation of RAD51 filaments through several consecutive association steps with proposed regulatory steps. See text for more details.

context of DNA stretching, competing non-homologous dsDNA, chromosome structure and perhaps orientation of the major and minor grooves of dsDNA with respect to the incoming pre-synaptic complex (41). It is likely that efficient and accurate strand exchange with homologous dsDNA involves specific, dynamic and structural changes in pre-synaptic complexes and dsDNA. Secondly, it has been proposed that homology search within the context of genomic dsDNA may be more efficient if the pre-synaptic complex contains gaps or structural discontinuities due to the ability of distinct sub-divisions of the pre-synaptic complex to reduce the complexity of homology search (42).

We also extended our study to bacterial and yeast recombinases to understand possible evolutionary aspects of NF regulation. While bacterial RecA, yeast Rad51 and human RAD51 recombinases are each critical for promoting strand exchange, our study reveals unexpected differences. For instance, the ATPase activity of RecA is known to be much higher than that of human RAD51 (43,44). Here we demonstrate that while RecA shows strong DNA binding at all nucleotide states, yRad51 exhibits a striking nucleotide dependence ranging from weak binding in apo condition, through cooperative binding in AMP-PNP to strong binding in the presence of ATP. In addition, rapid ATP binding by yRad51 that precedes and enhances the binding of the protein to ssDNA further highlight a difference from the human protein, which can bind DNA rapidly in the absence of nucleotide and subsequently undergo an ATP-dependent isomerization after filament assembly. Notably, we previously showed that *C. elegans* RAD-51 behaves similarly to yeast Rad51 in this regard (3). Post-translational modification or interaction with RAD51 binding partners could influence its properties (Figure 7). The importance of such regulation was shown for yeast Rad51 where mutations of the Walker A box residue Ser 192, which can undergo phosphorylation, leads to loss of ATP hydrolysis and also DNA binding (45). Interestingly, Tyr 54 phosphorylation of human RAD51 enhances its DNA strand exchange activity by altering the nucleoprotein filament properties (38).

Even more striking is the correlation between inherent recombinase complexity and the diversity of regulatory mechanisms in promoting filament assembly. We propose that filament assembly/disassembly are complex multiphase processes that can be regulated by nucleotide co-factors and HR regulators. Each state may represent a potential regulatory point where different RAD51-interacting proteins could influence the properties of the NFs (Figure 7). In *E. coli*, few recombination mediators have been described, with the RecFOR complex playing a major role (35). While in *S. cerevisiae* yRad51 is targeted to ssDNA by yRad52, in human cells BRCA2 serves as the main recombination mediator. Interestingly, *C. elegans* BRC-2 (46) and human BRCA2 (47,48), inhibit the ATPase activity of RAD51 and also directly interact with RAD51-ssDNA filaments as well as with free RAD51. Whereas RecFOR and yRad52 do not inhibit ATP hydrolysis of RecA and yRad51, respectively (35,49). Thus, in addition to promoting NF assembly, BRCA2 may also stabilize nascent RAD51 NFs by locking the filaments in a strong DNA-binding mode providing another layer of RAD51 regulation unique to metazoans. In addition, we have shown that RAD51 paralogs from *C. elegans* remodel presynaptic filaments into more 'open' flexible and stable conformation (3) and HOP2-MND1 or the Shu complex could promote active NF assembly at different

stages of the multiphasic assembly profile (50,51). Observations that BCCIPβ induces a conformational change within the RAD51 NF that promotes release of ADP to help maintain an active presynaptic filament (52) support our conclusion.

The differences in filament dissociation kinetics among different species could also be relevant to different strategies of negative HR control at the level of the pre-synaptic NF. In bacteria, turnover of RecA from ssDNA relies heavily on its intrinsic ATPase activity (35), which is very strong compared to yeast (53) and mammalian recombinases (44). In *Saccharomyces cerevisiae*, the Srs2 anti-recombinase actively dismantles Rad51 NF (35) in part by the activation of yRad51-catalyzed ATP hydrolysis upon physical interaction with Srs2 (26). Intrinsic RecA and yRad51 filament disassembly observed in the presence of either ADP or ATP strongly support these findings. However, the situation is strikingly different in humans, where both *in vitro* and *in vivo* multiple anti-recombinases could dismantle RAD51 filaments, including PARI (54), FBH1 (55), RECQ5 (56) and BLM (57). While PARI appears to be functionally similar to Srs2 and may promote RAD51 ATP hydrolysis and NF turnover, the FBH1 and RECQ5 helicases actively and specifically disrupt the presynaptic filament without activating ATP hydrolysis by RAD51. Indeed, our findings suggest that although human RAD51 NFs are intrinsically very dynamic, they are nevertheless more stable in any nucleotide-bound state, thus indicating that the antirecombinase-mediated ATPase stimulation is likely to be insufficient to drive NF turnover. It is possible that FBH1 and RECQ5 preferentially disrupt different NF intermediates or nucleotide-bound states observed for human RAD51 NF disassembly.

The embryonic lethality associated with RAD51 depletion as well as the reported phenotypes of Walker box and Fanconi anemia (FA)-associated RAD51 mutants indicate that aberrant RAD51 filament structures represent serious threats to genomic stability and cell survival. A recent high-resolution cryo-EM structure (20) highlighted the possibility of two newly described FA-associated RAD51 mutations directly or indirectly disrupting the Walker box motifs, resulting in defective NF assembly (58,59). Indeed, both mutations induce structural changes and filament destabilization by prevention of ATP hydrolysis due to defective or aberrant ATP binding (60). Also, recently described cancer-associated RAD51 mutations have been shown to alter physical properties of the recombinase, with one such mutant leading to a hyper-recombination phenotype (61). Finally, mutations in RAD51-interacting partners such as the RAD51 paralogs are associated with predisposition to breast and ovarian cancer (62). The exact molecular mechanism of how human RAD51 paralogs influence RAD51 is not well understood. It is intriguing to speculate that their mutations might in turn aberrantly alter NF function.

In summary, our work provides the first description of unexpected intrinsic properties of RAD51 filament behavior over a millisecond time-scale that could allow not only mechanistic understanding of the underlying mechanisms of genome instability associated with defects in RAD51 and its interacting partners, but provide also potential therapeutic opportunities.

SUPPLEMENTARY DATA

Supplementary Data are available at NAR Online.

ACKNOWLEDGEMENTS

We thank Simon Boulton, Eric Greene, Petr Cejka and Martin Taylor for discussions and comments on the manuscript. CIISB research infrastructure project LM2015043 funded by MEYS CR is gratefully acknowledged for the financial support of the measurements at the Cryo-electron Microscopy and Tomography core facility. Access to computing and storage facilities owned by parties and projects contributing to the National Grid Infrastructure MetaCentrum, provided under the programme 'Projects of Large Research, Development, and Innovations Infrastructures' (CESNET LM2015042), is greatly appreciated. We thank M. Peterek for cryo-EM data collection.

FUNDING

Czech Science Foundation [17-17720S]; Wellcome Trust Collaborative Grant [206292/E/17/Z]; and National Program of Sustainability II [MEYS CR, project no. LQ1605] to L.K. Laboratory; Human Frontier Science Program [RGY0072/2010]; 'Momentum' Program of the Hungarian Academy of Sciences [LP2011-006/2011, NKFIH K-116072, NKFIH ERC_HU 117680 to M.K. Laboratory]; Marie Sklodowska-Curie Reintegration Fellowship [H2020-MSCA-IF-2014-657076 to M.G.]; Premium Postdoctoral Program of the Hungarian Academy of Sciences [PPD-017/2017 to G.M.H.]; Funding for open access charge: Grantová Agentura České Republiky.
Conflict of interest statement. None declared.

REFERENCES

1. Krejci,L., Altmannova,V., Spirek,M. and Zhao,X. (2012) Homologous recombination and its regulation. *Nucleic Acids Res.*, **40**, 5795–5818.
2. San Filippo,J., Chi,P., Sehorn,M.G., Etchin,J., Krejci,L. and Sung,P. (2006) Recombination mediator and Rad51 targeting activities of a human BRCA2 polypeptide. *J. Biol. Chem.*, **281**, 11649–11657.
3. Taylor,M.R., Špírek,M., Chaurasiya,K.R., Ward,J.D., Carzaniga,R., Yu,X., Egelman,E.H., Collinson,L.M., Rueda,D., Krejci,L. *et al.* (2015) Rad51 paralogs remodel pre-synaptic Rad51 filaments to stimulate homologous recombination. *Cell*, **162**, 271–286.
4. Gaines,W.A., Godin,S.K., Kabbinavar,F.F., Rao,T., VanDemark,A.P., Sung,P. and Bernstein,K.A. (2015) Promotion of presynaptic filament assembly by the ensemble of S. cerevisiae Rad51 paralogues with Rad52. *Nat. Commun.*, **6**, 7834.
5. Chapman,J.R., Taylor,M.R. and Boulton,S.J. (2012) Playing the end game: DNA double-strand break repair pathway choice. *Mol. Cell*, **47**, 497–510.
6. Hilario,J., Amitani,I., Baskin,R.J. and Kowalczykowski,S.C. (2009) Direct imaging of human Rad51 nucleoprotein dynamics on individual DNA molecules. *Proc. Natl Acad. Sci. U.S.A.*, **106**, 361–368.
7. van der Heijden,T., Seidel,R., Modesti,M., Kanaar,R., Wyman,C. and Dekker,C. (2007) Real-time assembly and disassembly of human RAD51 filaments on individual DNA molecules. *Nucleic Acids Res.*, **35**, 5646–5657.
8. Candelli,A., Holthausen,J.T., Depken,M., Brouwer,I., Franker,M.A., Marchetti,M., Heller,I., Bernard,S., Garcin,E.B., Modesti,M. *et al.* (2014) Visualization and quantification of nascent RAD51 filament formation at single-monomer resolution. *Proc. Natl Acad. Sci. U.S.A.*, **111**, 15090–15095.

9. Sigurdsson,S., Trujillo,K., Song,B., Stratton,S. and Sung,P. (2001) Basis for avid homologous DNA strand exchange by human Rad51 and RPA. *J. Biol. Chem.*, **276**, 8798–8806.
10. Van Komen,S., Macris,M., Sehorn,M.G. and Sung,P. (2006) Purification and assays of Saccharomyces cerevisiae homologous recombination proteins. *Methods Enzymol.*, **408**, 445–463.
11. Lusetti,S.L., Wood,E.A., Fleming,C.D., Modica,M.J., Korth,J., Abbott,L., Dwyer,D.W., Roca,A.I., Inman,R.B. and Cox,M.M. (2003) C-terminal deletions of the Escherichia coli RecA protein. Characterization of in vivo and in vitro effects. *J. Biol. Chem.*, **278**, 16372–16380.
12. Rohou,A. and Grigorieff,N. (2015) CTFFIND4: Fast and accurate defocus estimation from electron micrographs. *J. Struct. Biol.*, **192**, 216–221.
13. Tang,G., Peng,L., Baldwin,P.R., Mann,D.S., Jiang,W., Rees,I. and Ludtke,S.J. (2007) EMAN2: an extensible image processing suite for electron microscopy. *J. Struct. Biol.*, **157**, 38–46.
14. Scheres,S.H. (2012) A Bayesian view on cryo-EM structure determination. *J. Mol. Biol.*, **415**, 406–418.
15. Egelman,E.H. (2000) A robust algorithm for the reconstruction of helical filaments using single-particle methods. *Ultramicroscopy*, **85**, 225–234.
16. Yu,X., Jacobs,S.A., West,S.C., Ogawa,T. and Egelman,E.H. (2001) Domain structure and dynamics in the helical filaments formed by RecA and Rad51 on DNA. *Proc. Natl. Acad. Sci. U.S.A.*, **98**, 8419–8424.
17. Pettersen,E.F., Goddard,T.D., Huang,C.C., Couch,G.S., Greenblatt,D.M., Meng,E.C. and Ferrin,T.E. (2004) UCSF Chimera—a visualization system for exploratory research and analysis. *J. Comput. Chem.*, **25**, 1605–1612.
18. Schindelin,J., Arganda-Carreras,I., Frise,E., Kaynig,V., Longair,M., Pietzsch,T., Preibisch,S., Rueden,C., Saalfeld,S., Schmid,B. *et al.* (2012) Fiji: an open-source platform for biological-image analysis. *Nat. Methods*, **9**, 676–682.
19. Ogawa,T., Yu,X., Shinohara,A. and Egelman,E.H. (1993) Similarity of the yeast RAD51 filament to the bacterial RecA filament. *Science*, **259**, 1896–1899.
20. Short,J.M., Liu,Y., Chen,S., Soni,N., Madhusudhan,M.S., Shivji,M.K. and Venkitaraman,A.R. (2016) High-resolution structure of the presynaptic RAD51 filament on single-stranded DNA by electron cryo-microscopy. *Nucleic Acids Res.*, **44**, 9017–9030.
21. Xu,J., Zhao,L., Xu,Y., Zhao,W., Sung,P. and Wang,H.W. (2017) Cryo-EM structures of human RAD51 recombinase filaments during catalysis of DNA-strand exchange. *Nat. Struct. Mol. Biol.*, **24**, 40–46.
22. Chi,P., Van Komen,S., Sehorn,M.G., Sigurdsson,S. and Sung,P. (2006) Roles of ATP binding and ATP hydrolysis in human Rad51 recombinase function. *DNA Repair (Amst.)*, **5**, 381–391.
23. Schay,G., Borka,B., Kernya,L., Bulyáki,É., Kardos,J., Fekete,M. and Fidy,J. (2016) Without Binding ATP, Human Rad51 Does Not Form Helical Filaments on ssDNA. *J. Phys. Chem. B*, **120**, 2165–2178.
24. Yu,X. and Egelman,E.H. (2010) Helical filaments of human Dmc1 protein on single-stranded DNA: a cautionary tale. *J. Mol. Biol.*, **401**, 544–551.
25. Hwang,H. and Myong,S. (2014) Protein induced fluorescence enhancement (PIFE) for probing protein-nucleic acid interactions. *Chem. Soc. Rev.*, **43**, 1221–1229.
26. Antony,E., Tomko,E.J., Xiao,Q., Krejci,L., Lohman,T.M. and Ellenberger,T. (2009) Srs2 disassembles Rad51 filaments by a protein-protein interaction triggering ATP turnover and dissociation of Rad51 from DNA. *Mol. Cell*, **35**, 105–115.
27. Tombline,G., Heinen,C.D., Shim,K.S. and Fishel,R. (2002) Biochemical characterization of the human RAD51 protein. III. Modulation of DNA binding by adenosine nucleotides. *J. Biol. Chem.*, **277**, 14434–14442.
28. Bugreev,D.V. and Mazin,A.V. (2004) Ca2+ activates human homologous recombination protein Rad51 by modulating its ATPase activity. *Proc. Natl. Acad. Sci. U.S.A.*, **101**, 9988–9993.
29. Forget,A.L., Loftus,M.S., McGrew,D.A., Bennett,B.T. and Knight,K.L. (2007) The human Rad51 K133A mutant is functional for DNA double-strand break repair in human cells. *Biochemistry*, **46**, 3566–3575.
30. Krejci,L., Van Komen,S., Li,Y., Villemain,J., Reddy,M.S., Klein,H., Ellenberger,T. and Sung,P. (2003) DNA helicase Srs2 disrupts the Rad51 presynaptic filament. *Nature*, **423**, 305–309.
31. Veaute,X., Jeusset,J., Soustelle,C., Kowalczykowski,S.C., Le Cam,E. and Fabre,F. (2003) The Srs2 helicase prevents recombination by disrupting Rad51 nucleoprotein filaments. *Nature*, **423**, 309–312.
32. Schlacher,K., Christ,N., Siaud,N., Egashira,A., Wu,H. and Jasin,M. (2011) Double-strand break repair-independent role for BRCA2 in blocking stalled replication fork degradation by MRE11. *Cell*, **145**, 529–542.
33. Galletto,R., Amitani,I., Baskin,R.J. and Kowalczykowski,S.C. (2006) Direct observation of individual RecA filaments assembling on single DNA molecules. *Nature*, **443**, 875–878.
34. Shahid,T., Soroka,J., Kong,E.H., Malivert,L., McIlwraith,M.J., Pape,T., West,S.C. and Zhang,X. (2014) Structure and mechanism of action of the BRCA2 breast cancer tumor suppressor. *Nat. Struct. Mol. Biol.*, **21**, 962–968.
35. Bell,J.C., Plank,J.L., Dombrowski,C.C. and Kowalczykowski,S.C. (2012) Direct imaging of RecA nucleation and growth on single molecules of SSB-coated ssDNA. *Nature*, **491**, 274–278.
36. Defais,M., Phez,E. and Johnson,N.P. (2003) Kinetic mechanism for the formation of the presynaptic complex of the bacterial recombinase RecA. *J. Biol. Chem.*, **278**, 3545–3551.
37. Paulus,B.F. and Bryant,F.R. (1997) Time-dependent inhibition of recA protein-catalyzed ATP hydrolysis by ATPgammaS: evidence for a rate-determining isomerization of the recA-ssDNA complex. *Biochemistry*, **36**, 7832–7838.
38. Subramanyam,S., Ismail,M., Bhattacharya,I. and Spies,M. (2016) Tyrosine phosphorylation stimulates activity of human RAD51 recombinase through altered nucleoprotein filament dynamics. *Proc. Natl. Acad. Sci. U.S.A.*, **113**, E6045–E6054.
39. Ristic,D., Modesti,M., van der Heijden,T., van Noort,J., Dekker,C., Kanaar,R. and Wyman,C. (2005) Human Rad51 filaments on double- and single-stranded DNA: correlating regular and irregular forms with recombination function. *Nucleic Acids Res.*, **33**, 3292–3302.
40. Kim,T.M., Ko,J.H., Hu,L., Kim,S.A., Bishop,A.J., Vijg,J., Montagna,C. and Hasty,P. (2012) RAD51 mutants cause replication defects and chromosomal instability. *Mol. Cell. Biol.*, **32**, 3663–3680.
41. Greene,E.C. (2016) DNA sequence alignment during homologous recombination. *J. Biol. Chem.*, **291**, 11572–11580.
42. Qi,Z., Redding,S., Lee,J.Y., Gibb,B., Kwon,Y., Niu,H., Gaines,W.A., Sung,P. and Greene,E.C. (2015) DNA sequence alignment by microhomology sampling during homologous recombination. *Cell*, **160**, 856–869.
43. Kowalczykowski,S.C. and Krupp,R.A. (1987) Effects of Escherichia coli SSB protein on the single-stranded DNA-dependent ATPase activity of Escherichia coli RecA protein. Evidence that SSB protein facilitates the binding of RecA protein to regions of secondary structure within single-stranded DNA. *J. Mol. Biol.*, **193**, 97–113.
44. Tombline,G. and Fishel,R. (2002) Biochemical characterization of the human RAD51 protein. I. ATP hydrolysis. *J. Biol. Chem.*, **277**, 14417–14425.
45. Flott,S., Kwon,Y., Pigli,Y.Z., Rice,P.A., Sung,P. and Jackson,S.P. (2011) Regulation of Rad51 function by phosphorylation. *EMBO Rep.*, **12**, 833–839.
46. Petalcorin,M.I., Galkin,V.E., Yu,X., Egelman,E.H. and Boulton,S.J. (2007) Stabilization of RAD-51-DNA filaments via an interaction domain in Caenorhabditis elegans BRCA2. *Proc. Natl Acad. Sci. U.S.A.*, **104**, 8299–8304.
47. Carreira,A., Hilario,J., Amitani,I., Baskin,R.J., Shivji,M.K., Venkitaraman,A.R. and Kowalczykowski,S.C. (2009) The BRC repeats of BRCA2 modulate the DNA-binding selectivity of RAD51. *Cell*, **136**, 1032–1043.
48. Jensen,R.B., Carreira,A. and Kowalczykowski,S.C. (2010) Purified human BRCA2 stimulates RAD51-mediated recombination. *Nature*, **467**, 678–683.
49. Shinohara,A. and Ogawa,T. (1998) Stimulation by Rad52 of yeast Rad51-mediated recombination. *Nature*, **391**, 404–407.
50. Chi,P., San Filippo,J., Sehorn,M.G., Petukhova,G.V. and Sung,P. (2007) Bipartite stimulatory action of the Hop2-Mnd1 complex on the Rad51 recombinase. *Genes Dev.*, **21**, 1747–1757.
51. Sasanuma,H., Tawaramoto,M.S., Lao,J.P., Hosaka,H., Sanda,E., Suzuki,M., Yamashita,E., Hunter,N., Shinohara,M., Nakagawa,A.

et al. (2013) A new protein complex promoting the assembly of Rad51 filaments. *Nat Commun*, **4**, 1676.
52. Kelso,A.A., Goodson,S.D., Watts,L.E., Ledford,L.L., Waldvogel,S.M., Diehl,J.N., Shah,S.B., Say,A.F., White,J.D. and Sehorn,M.G. (2017) The β-isoform of BCCIP promotes ADP release from the RAD51 presynaptic filament and enhances homologous DNA pairing. *Nucleic Acids Res.*, **45**, 711–725.
53. Sung,P. (1994) Catalysis of ATP-dependent homologous DNA pairing and strand exchange by yeast RAD51 protein. *Science*, **265**, 1241–1243.
54. Moldovan,G.L., Dejsuphong,D., Petalcorin,M.I., Hofmann,K., Takeda,S., Boulton,S.J. and D'Andrea,A.D. (2012) Inhibition of homologous recombination by the PCNA-interacting protein PARI. *Mol. Cell*, **45**, 75–86.
55. Simandlova,J., Zagelbaum,J., Payne,M.J., Chu,W.K., Shevelev,I., Hanada,K., Chatterjee,S., Reid,D.A., Liu,Y., Janscak,P. *et al.* (2013) FBH1 helicase disrupts RAD51 filaments in vitro and modulates homologous recombination in mammalian cells. *J. Biol. Chem.*, **288**, 34168–34180.
56. Hu,Y., Raynard,S., Sehorn,M.G., Lu,X., Bussen,W., Zheng,L., Stark,J.M., Barnes,E.L., Chi,P., Janscak,P. *et al.* (2007) RECQL5/Recql5 helicase regulates homologous recombination and suppresses tumor formation via disruption of Rad51 presynaptic filaments. *Genes Dev.*, **21**, 3073–3084.
57. Bugreev,D.V., Yu,X., Egelman,E.H. and Mazin,A.V. (2007) Novel pro- and anti-recombination activities of the Bloom's syndrome helicase. *Genes Dev.*, **21**, 3085–3094.
58. Wang,A.T., Kim,T., Wagner,J.E., Conti,B.A., Lach,F.P., Huang,A.L., Molina,H., Sanborn,E.M., Zierhut,H., Cornes,B.K. *et al.* (2015) A dominant mutation in human RAD51 reveals its function in DNA interstrand crosslink repair independent of homologous recombination. *Mol. Cell*, **59**, 478–490.
59. Ameziane,N., May,P., Haitjema,A., van de Vrugt,H.J., van Rossum-Fikkert,S.E., Ristic,D., Williams,G.J., Balk,J., Rockx,D., Li,H. *et al.* (2015) A novel Fanconi anaemia subtype associated with a dominant-negative mutation in RAD51. *Nat Commun*, **6**, 8829.
60. Zadorozhny,K., Sannino,V., Beláň,O., Mlčoušková,J., Špírek,M., Costanzo,V. and Krejčí,L. (2017) Fanconi-anemia-associated mutations destabilize RAD51 filaments and impair replication fork protection. *Cell Rep.*, **21**, 333–340.
61. Marsden,C.G., Jensen,R.B., Zagelbaum,J., Rothenberg,E., Morrical,S.W., Wallace,S.S. and Sweasy,J.B. (2016) The tumor-associated variant RAD51 G151D induces a hyper-recombination phenotype. *PLos Genet.*, **12**, e1006208.
62. Godin,S.K., Sullivan,M.R. and Bernstein,K.A. (2016) Novel insights into RAD51 activity and regulation during homologous recombination and DNA replication. *Biochem. Cell. Biol.*, **94**, 407–418.